A Display Framework for Visualizing Real-Time 3D Lung Tumor Radiotherapy

Anand P. Santhanam, *Member, IEEE*, Twyla R. Willoughby, Ilhan Kaya, Amish P. Shah, Sanford L. Meeks, Jannick P. Rolland, *Senior Member, IEEE*, and Patrick A. Kupelian

(Invited Paper)

***Abstract*—Medical display systems are valuable tools in enabling the clinicians in the field of radiation therapy to view a patient's multi-modal information and treatment plan details. The effectiveness of display systems is further improved by including computer-based visualization systems that deliver the content comprehensively. In this paper, we present a medical display and visualization framework for radiation therapy that couples a computer-based simulation of real-time lung tumor motion and its dose accumulation during treatment with an Augmented Reality Center (ARC) based display system. The simulation framework provides insights on the variations in the effectiveness of the lung therapy for changes in the patient's breathing conditions. The display system aims to enhance the clinician's understanding by enhancing the 3D depth perception of the dose accumulation in lung tumors. Thus the framework acts as a tool for presenting both pre-operative studies and intra-operative treatment efficacy analysis when coupled with a real-time respiration monitor. A first evaluation of this framework was carried out using six clinical experts. Results show that, using the ARC compared to a 2D monitor, the experts were able to more efficiently perceive the radiation dose delivered to various aspects of the moving tumor and the surrounding normal tissues, as well as more quickly detecting radiation hot spots that are critical to minimizing damage to healthy tissue.**

***Index Terms*—Film dosimetry, medical visualization, 3D modeling.**

I. Introduction

MEDICAL display systems are effective in conveying clinically significant data related to a patient's pre-operative, intra-operative, and post-operative intervention procedures. They are critical in visualizing multi-modal images and their analysis. Of particular importance is the role of medical displays in radiotherapy. Recent advancements in imaging modalities have led to the availability of high-resolution 3D and 4D images of patients. Medical display systems allow a clinician to segment organs and tumors from these images with less than a 3-mm error and to plan a subject-specific treatment procedure. Once planned, the results of the radiation dose delivered to the tumor and the surrounding organs are also displayed and visually analyzed by the clinician.

The choice of a display system can be optimized based on the display content. While 2D display systems such as LCD monitors are effective in presenting 2D slices of CT and other imaging modalities, 3D display systems present the promise to be effective in presenting 3D segmented data-sets and their dynamics [1].

The focus of the current work is to enhance the 3D visualization of radiation therapy for lung tumors. Lung tumors move unpredictably, in 3D, and the motion specifics depend on the patient's body orientation and physiological condition. Such a complex tumor motion subsequently compromises the accurate deposition of radiation doses. The goal in radiation therapy is to deliver a high dose to a tumor, while sparing normal tissue. Most dose calculations and evaluations of a planned course of treatment are performed on 3D CT images of the patient taken prior to treatment. These images are usually high quality 3D CT scans so that the physician, physicists, and dosimetrists can identify normal structures to be spared from radiation and the tumor and other involved tissue that must be targeted. While the dosimetry methods using 3D CT images are accurate in representing the physics of the radiation interactions, there remains a major concern that the CT images that are used for these calculations do not adequately represent the patient anatomy at the time of radiation treatment. The variations in the patient position from day to day (setup uncertainties), as well as internal changes from day to day (inter-fraction motion), and internal changes during a single radiation treatment (intrafraction), have led to using a larger target volume than what is visualized on the CT images to ensure adequate coverage of the target [2].

In recent studies, 4DCT scans or multiple CT scans at different phases of the respiratory cycle have been used to assess the range of target motion and to more adequately define the margins for motion [3]. Once the target motion has been described, a dose model may be able to combine the probability distribution of the target motion with the treatment machine's pencil beam fluence to calculate dose [4]–[6]. These calculations, although accurate for the CT scan on which they are calcu-

Manuscript received February 08, 2008; revised May 11, 2008. First published September 30, 2008; current version published November 19, 2008. This work was supported by Calypso Medical, Seattle, WA, by MD Anderson Cancer Center, Orlando, FL, and the University of Central Florida under UCF I4 Corridor Program.

A. P. Santhanam is with the College of Optics and Photonics, University of Central Florida, Orlando, FL 32816 USA (e-mail: asanthan@mail.ucf.edu).

T. R. Willoughby, A. P. Shah, S. L. Meeks, and P. A. Kupelian are with the MD Anderson Cancer Center, Orlando, FL 32806 USA (e-mail: Twyla.willoughby@orhs.org; Amish.shah@orhs.org; Sanford.meeks@orhs.org; Patrick.kupelian@orhs.org).

I. Kaya is with the College of Engineering and Computer Science at the University of Central Florida, Orlando, FL 32806 USA (e-mail: ilhan@odalab.ucf.edu).

J. P. Rolland is with the College of Optics and Photonics, the College of Medicine, and the College of Engineering at the University of Central Florida, Orlando, FL 32816 USA (e-mail: jannick@odalab.ucf.edu).

Color versions of one or more figures are available online at http://ieeexplore.ieee.org.

Digital Object Identifier 10.1109/JDT.2008.2003343

lated, are still not optimal because of the breathing variations in lungs during treatment. 3D physics and physiology based simulations of lung tumor motion may assist in predicting the radiation dose accumulation during treatment. The effectiveness is further enhanced when the dose accumulated on a lung tumor is visualized in 3D. The different levels of dose accumulated are color-coded as traditionally viewed in the field of dosimetry. ARC enables visualizing the color-coded lung tumor dose in 3D, which facilitates for the clinicians the understanding of the treatment delivery on the patient's anatomy and helps them assess the expected treatment efficacy.

This paper discusses the ARC display coupled to a visualization framework tailored for the 3D conformal lung tumor dosimetry. Specifically, a real-time simulation method to calculate the delivered dose to various aspects of the moving lung tumor during the delivery of radiation is integrated into the ARC 3D visualization display. To date, delivery of radiation therapy is done without any such assessment of the dosimetric accuracy of the delivered doses at the time of the actual delivery of radiation. The proposed methods and visualization framework discuss an integration of lung tumor motion simulation and ARC-based 3D display system, which will be used for the first time in clinical radiotherapy. In Section II, we shall review related work in the field of moving tumor dosimetry, which forms the content for the 3D display technology. It is followed by a brief discussion of current 3D display technologies. In Section III, methods of imaging, simulated lung dynamics and associated tumor motion, capturing of the patient breathing cycle, and treatment planning and dosimetry are presented. Results of the simulation framework are given in Section IV. Finally, an evaluation of this framework using six clinical experts is presented in Section V, where clinicians visualize the radiation dose delivery on a tumor and surrounding tissues and look for hot spots outside the lung tumor. Such visualization enables experts to decide whether the radiation delivery should be aborted based on the 3D location of the hot spot formation. Section VI concludes the paper.

II. Related Work

A. Moving Tumor Dosimetry

Moving tumor dosimetry has been previously studied using two approaches, namely: 1) 4DCT-based studies and 2) phantom-based studies.

1) 4DCT Based Studies: There have been many studies to evaluate the motion of a lung tumor for radiation therapy. The imaging modality of 4DCT facilitates the availability of the patient specific lung tumor motion details. A detailed discussion on the usage of 4DCT for predicting tumor motion is given in the report of the AAPM Task-Group 76 (TG 76) [7]. The methods are however limited by the fact that they do not account for tumor motion variations caused by variations in breathing such as rib-cage diaphragm compensation, changes in lung ventilation, and inter-fraction modifications in the patient anatomy.

2) Phantom Based Studies: Phantom work is usually done in the field of medical physics to perform a start to finish planning and delivery of the same type of radiation delivery that will be given to a patient. Phantom work has been used in the past to optimize the 4DCT scanning parameters to better model patient motion [8]. For the specific application of radiation dosimetry, phantom work has been used to determine the effects of motion on particular radiation delivery. Early work of assessing the effects of motion on radiation was summarized in the TG 76 report and has been reported in several different studies [9]. These methods of evaluating the effects of motion on a radiation delivery have been performed with simplistic motion phantoms that move in 1D and with either point measuring devices such as ion chambers or film.

Another utilization of phantom measurements has been to validate different treatment techniques or dose calculation methods [10]–[12]. As these techniques continue to be reported in the literature, there are more sophisticated phantoms that are being developed where the physical parameters of patient deformation can be modeled. A programmable 4D phantom has been developed that can be programmed to move based on an actual patient motion signal. Another phantom that is reported in the literature can provide simple deformations to model lung breathing [13].

B. 3D Displays

3D display systems have been extensively investigated and developed for catering applications in fields ranging from entertainment to manufacturing. These display systems can be broadly classified into three types: 1) Volumetric displays; 2) auto-stereoscopic displays; and 3) stereoscopic displays. Each of these display systems has its own advantages and limitations.

Volumetric displays are based on physical mechanisms that display points of light within a volume. Such display systems use either multi-planar display panels or single rotating display panel for rendering a given 3D content. These display systems effectively overcome the limitations imposed by the 2D display panels on visualizing the 3D content. A detailed discussion on volumetric displays is provided in this special issue by [14], as well as a novel display system aimed at visualizing radiation oncology treatment plans. The development of volumetric display systems, which are currently limited by the size and resolution of the actual 3D content, is an active area of research. Such displays provide a natural setting for multiple user use, yet what is being displayed to each user is limited to one view of the 3D content.

Autostereoscopic displays are based on physical mechanisms that display 2D projections of the 3D content that vary for different viewing angles. Lenticular lenses and parallax barriers are used to achieve a view-angle based rendering. These techniques are partly effective in representing the 3D content and are intrinsically limited in providing the actual depth cues.

Stereoscopic displays such as head-worn displays (HWDs) provide a 3D rendering for each eye. Such displays [15] have the ability to provide 3D views with realistic depth cues. Such display systems to date have a higher resolution, color capability, depth display capability, and mobility compared to volumetric displays [1]. Additionally, such display systems also cost-effectively support multi-user visualization with user-centric content, which is required for visualizing 3D lung tumor dose accumulation [16], [17]. For instance, a dosimetrist and clinician can view the 3D dose accumulation process with the dosimetrist viewing the dose distribution while the clinician is viewing the normal tissue tolerance. These displays are worn in a similar way people

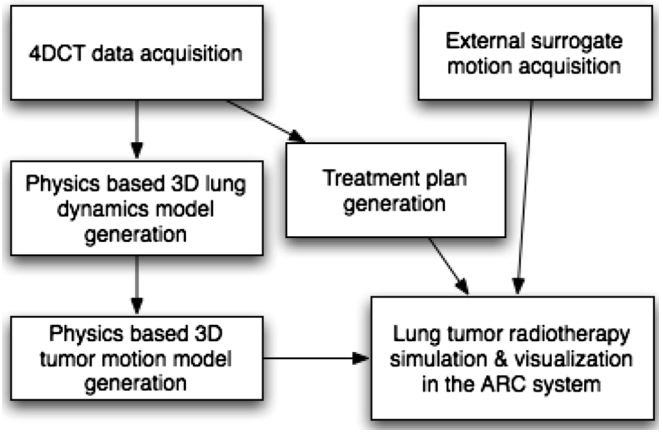

Fig. 1. A schematic diagram of the proposed display framework.

wear eye glasses. The challenge lies in the design of head-worn displays that are light weight (i.e. $<\sim$500 g) and provide sufficient field of view for the content and overall applications. In this paper, we investigate the feasibility of using the ARC display system that builds on head-worn projection optics of $\sim$6 g per eye, yet can achieve fields of views of at least 70 deg [18]. At least modest field of views of 40 deg are required for viewing the treatment plan delivery on a moving lung tumor.

III. Methods

In this paper, we discuss a framework that integrates a real-time simulation of lung tumor motion with a 3D display system. The real-time simulation of lung tumor motion takes into account the patient specific lung tumor motion extracted from 4DCT images and the radiation plan prescribed for the patient. The output of the simulation framework predicts the amount and location of radiation doses deposited in both moving lung tumors and surrounding normal lung tissues during the delivery of radiation. The dose collected in the lung tumor can be visualized in an ARC display system that allows multiple users to simultaneously view the color-coded 3D dose accumulation from different view angles. Another unique feature of the ARC display system is the ability it provides to interact with other ARC display systems connected through the network. Thus clinicians geographically separated can also interact and investigate the effectiveness of the patient's treatment plan taking into account the subject-specific lung motion and lung tumor motion.

Fig. 1 shows a schematic diagram of the proposed framework and the components are explained in this section as follows; We first discuss the steps involved in the 4DCT acquisition and their segmentation (Section III-A), the generation of deformable surface lung (Section III-B), and the lung tumor model (Section III-C). Next we discuss the steps involved in the respiration signal acquisition and their correlation (Section III-D). We then discuss the steps involved in developing a treatment plan using one of the 3D CT (Section III-E). It is followed by a discussion on the dose accumulation model (Section III-F). Section III-G presents a description of the ARC display system.

A. 4DCT Acquisition

For each patient, the collection of data for treatment planning included seven studies with multiple imaging modalities. The studies included a PET/CT scan, a 4DPET scan, a 4DCT scan, inhalation breath-hold, normal breathing scan, exhalation breath-hold, and the exhalation breath-hold scan with intravenous contrast. The selection of the scan region was dependent on the tumor volume and the treatment location. The tumor volume was localized by previously implanted gold fiducials (Visicoil markers). The 4DCT studies were acquired with a pitch of 1.0 and reconstructed in 3 mm slices. The CT acquisition technique chosen was the standard chest protocol. In order to improve the image quality, no CT dose restriction was used. The 4DCT data was acquired with the Siemens Biograph 64. The PET/CT system respiratory gated CT acquisition was performed with the Anzai AZ-733V strain-gauge system. The 4DCT data was reconstructed retrospectively and the phases were sorted in increments of every 10% of the strain-gauge signal, which represents the breathing cycle. These phases were automatically sorted following expert selection of the maximum inspiration and maximum end-expiration points of the respiratory cycle. The 3D lung models were segmented using OSIRIX segmentation software. The lung tumors were segmented manually in the Pinnacle treatment system and stored as a DICOM RT structure.

B. Physics and Physiology Based 3D Lung Surface Model

The estimation of a subject-specific deformation operator, first described in [19], is now summarized for the comprehensiveness of the paper. The estimation takes as input segmented 3D lung surface models obtained from the 4DCT of the patient. The segmented lung surface models are registered as shown in [20], [21] to compute the surface displacement. The general formula of the Green's function (GF) as an operator in discrete space is given as

$$x(I) = \sum_J K(J,I) \times f(J), \tag{1}$$

where $x(I)$ is the displacement of the node I, $f(J)$ is the force applied on node J, and $K(J,I)$ is the GF operator (deformation kernel) that represents the elastic interaction between nodes, taking into account both the inter-nodal distance and elastic properties. The elements of the kernel row represent the normalized weights of the force transferred from one node to others. From a mathematical perspective, solving for the kernel (as a matrix) is not possible since (1) in simultaneous form has more than one unknown per equation. However, from a physics perspective, we can further simplify the deformation kernel as now described.

Two general forms of the GF operator are now employed. In the first form, the GF operator can be written as

$$K(J,I) = C_I \cos z'(J,I) \tag{2}$$

where C_I is an arbitrary constant and $z'(J,I)$ is a function that returns a value in the range of 0to $\pi/2$. Equation (2) represents a row of the kernel matrix as a cosine function. The second form of the kernel row is described as a proportionality function of the piecewise Euclidean distance $d(J,I)$ between I and J [22], which can be written as

$$\cos\left(z'(J,I)\right) = \frac{1}{4\pi d'(J,I)}, \tag{3}$$

where $d'(J,I)$ is a function that takes into account both the Euclidean distance and the local elastic properties. It can be seen

that for higher values of $d'(J,I)$, the value of $K(J,I)$ tends to zero. An initial representation for $d'(J,I)$ is given as a linear combination of the distance and the elastic interaction

$$d'(J,I) = A_I d(J,I) + B_J e(J,I) \tag{4}$$

where A_I and B_I are arbitrary constants. These constants are also referred to as structural constants in this paper, since they both compute the function d'. The function $d(J,I)$ represents the Euclidean distance between the nodes J and I. The function $e(J,I)$ that represents the elastic interaction between nodes J and I is given as a difference in the alveolar expansion of the region surrounding nodes J and I. The function e is thus defined as

$$e(J,I) = a(J) - a(I) \tag{5}$$

where $a(J)$ is a function representing an estimated alveolar expandability in the region surrounding node J. It can be seen that the inverse lung deformation problem now mathematically relates to computing the values of A_I, B_I, and C_I for each node I.

The value of C_I can be computed by merging the deformation kernel's expansion given in (2) with (1). The value of C_I can now be written as

$$C_I = \frac{x(I)}{\sum_{J=0}^{N} f(J) \times \cos\left(z'(J,I)\right)}. \tag{6}$$

The steps involved in the generation of a deformable lung surface model are as follows: A 4DCT data is taken as input and the 3D lungs are segmented from each 3D CT of this dataset. A set of three 3D CT datasets is chosen for the estimation of the GF operator and the rest of the 3D CT datasets is used for validation. The 3D segmented lungs are then registered with each other using the ray projection method discussed in [20]. Once registered the value of $x(I)$ for every lung surface node is known. The applied force on each node is taken to be the vertical gradient of the lung surface node's position, which changes with the lung orientation. The GF operator is then estimated and validated by simulating lung deformation. The deformations are separately validated by comparing the simulated shapes for a given air volume with 3DCT snapshots at the same air volume. For the two 4DCTs that we considered, the deformations matched the 3DCT snapshots with approximately 2% RMS difference.

C. Physics Based 3D Lung Tumor Model

We now describe a method to compute subject specific lung tumor motion accounting for the subject-specific lung deformation operator estimated in Section III-B. This method is based on the assumption that the lung tumor acts as a single rigid body connected to the lung parenchyma. Since our deformable lung model only consists of the surface of the lung, an association is made between a point in the center of the tumor and the lung surface. We create a data structure that stores a surface node location and the angle of this surface node made from the center of the lung tumor. The data structure is populated by projecting a ray from the center of the tumor and computing a ray triangle intersection with the lung surface model. From a physics perspective, each of these rays represents a spring such that the tumor is connected to the lung surface by the springs. The closest node of intersection point is noted. Let $N(\theta,\vartheta)$ be the list of points. Let $d(N(\theta,\vartheta))$ be the normalized Euclidean distance between the center of the lung tumor and the surface node given by $N(\theta,\vartheta)$. The normalization factor in this case is the Euclidean distance between the center of the lung tumor and the farthest lung surface node, and $d(N(\theta,\vartheta))$ can be written as

$$d\left(N(\theta,\vartheta)\right) = 1 - \frac{d_e\left(N(\theta,\vartheta)\right)}{d_e^{\max}\left(N(\theta,\vartheta)\right)} \tag{7}$$

where d_e is the Euclidean distance between the center of the lung tumor and the surface node, and $d_e^{\max}$ is the Euclidean distance between the center of the lung tumor and the farthest lung surface node. Let L be an interpolation function that can be written as

$$L(\theta,\vartheta) = \frac{d^2\left(N(\theta,\vartheta)\right)}{d^2\left(N(\theta,\vartheta)\right) + d^2\left(N(\pi-\theta,\pi-\vartheta)\right)}. \tag{8}$$

It can be seen that the interpolation function is based on the Euclidean distance of the tumor center from two lung surface points given by $N(\theta,\vartheta)$ and $N(\pi-\theta,\pi-\vartheta)$. The displacement vector X_T of the lung tumor motion is computed from the displacement vector of the lung surface nodes $X(\theta,\vartheta)$ as

$$X_T = \frac{1}{N}\sum_{\theta=0}^{\pi}\sum_{\vartheta=0}^{2\pi} L(\theta,\vartheta)X(\theta,\vartheta) + L(\pi-\theta,\pi-\vartheta)X(\pi-\theta,\pi-\vartheta). \tag{9}$$

The above equation interpolates the position of the tumor with the surface movement given by the deformable lung model.

D. External Surrogates for Respiratory Motion

For radiation therapy, it is important to correlate the respiratory signals and tumor locations indicated by the various systems to make certain that the tumor motion is the same when imaged and during treatment. Measurement of the patient's breathing cycle can be acquired through several techniques. The following methodologies were available in our clinical setting: the Anzai Az-733V system (Tokyo, Japan), the Calypso 4D Localization System (Seattle, WA), and a spirometry desktop system developed by Cosmed Inc (Rome, Italy). With the Anzai respiratory gating system, an abdominal belt containing a strain gauge was wrapped around the patient's anterior surface, typically midway between the xyphoid process and the umbilicus. The exact position is chosen to maximize the AP respiratory-induced motion for the respiratory sensor. The Calypso System operates based on detection and localization of RF-emitting implanted Beacon transponders, allowing the 3D position of the implanted transponders and target isocenter to be determined at a frequency of 10 Hz. This is a real-time continuous localization of targets for external radiation therapy. With the turbine spirometer, measurements such as slow vital capacity (expiratory and inspiratory) can be recorded and saved. Slow vital capacity is the volume of gas measured on a slow, complete expiration after or before a maximal inspiration, without forced or rapid effort. None of these systems were invasive (in our use) and presented no possible risks (or inconveniences) to the patients. Additional monitoring procedures were not needed to ensure the safety of these patients. The tools that are used with these systems are external and do not

interfere with imaging or treatment. The patients that were recruited for this investigation were already under treatment using the Novalis ExacTrac System for respiratory gating.

We have compared the ability of three respiratory surrogates to mimic actual lung tumor motion during external beam radiotherapy. Since an important consideration in 4DCT imaging is the selection of a breathing metric for sorting the CT data and modeling internal motion, the correlation of the respiratory signals generated by the Siemens Anzai belt system with the signals generated by the Calypso system and the spirometry system was necessary. The Anzai system was used as the surrogate for 4DCT imaging and functioned as the standard between the three respiratory surrogates. We found that the Anzai system breathing signal representing the rib-cage diaphragm motion and the spirometry system's air volume signal were highly correlated (less than 2% difference with the spirometry) in measuring the patient's breathing cycle. The Calypso markers and the Anzai system were then correlated in order to account for the subject's rib-cage movements that are taken as input by the lung deformation model. The Calypso markers were place on the Anzai abdominal belt. The Anzai system and the Calypso markers (measuring motion in the anterior/posterior direction) were correlated to obtain the 3D anterior/posterior rib-cage motion. Work is currently being done to verify the correlation for a wide range of patients.

E. Treatment Planning System

For the purpose of treatment planning, we fused several phases from the 4DCT scan as well as a breath-hold CT from the image acquisition scheme using the Pinnacle treatment planning software. With the availability of the multiple dataset fusion, several gross tumor volumes (GTVs) were then drawn from the 4DCT data, with the end result being that an internal target volume (ITV) was drawn. This ITV compares the multiple GTVs but is mainly based on the end-expiration phase from the 4DCT scan and the exhale breath-hold CT scan. This method is similar to published studies where the maximum intensity projection (MIP) is generated from 4DCT datasets and used to delineate an ITV for all phases in the breathing cycle. Following expansion of the ITV to a new PTV (planning target volume), the contours were then sent to the treatment planning station for planning the gated treatment delivery. Studies have been done at our institution to evaluate optimal lung treatment planning for highly conformal and high dose fractionations. We have developed an in-house protocol for stereotactic body radiotherapy of lung tumors that delivers the entire treatment in a single session. As part of the preliminary work for this protocol, multiple treatment plans were developed to ensure that conformal beams could be aimed at the tumor that would provide adequate sparing of the normal tissues. In this planning exercise the iPlan software from BrainLab was used since this is the clinical system used to treat small lung tumors. Plans were generated on ten patients who had undergone radiation therapy. For this planning exercise the goal was to deliver a dose of 40 Gy minimum to the edge of the target on a single CT scan with no margin. For this purpose no tumor motion was accounted for either by the CT scans or for margins for motion during delivery. It was also assumed that the target could very accurately be localized at the time of treatment. In all cases the target coverage was adequate and all normal tissues and organs at risk were below the acceptable levels of approximately 20% of prescribed dose.

F. 3D Dosimetry Simulation Framework

We now discuss the simulation framework that integrates the 3D deformable lung model (Section III-B) and the lung tumor motion (Section III-C) with the treatment plan developed for the patient (Section III-E). The simulation framework consists of a virtual cuboid of dimension $100 \times 100 \times 100$ cubes created with each cube of the dimension $1 \times 1 \times 1$ mm^3. A 3D sphere representing the lung tumor is then introduced in the virtual cuboid. The position of this 3D sphere is based on the lung tumor position. The sphere is modeled to move based on the lung surface movement, as described in Section III-C. For most lung treatments, between six and nine conformal beams are aimed at the target.

1) Dose Accumulation Computation: The dose matrix computed from the iPlan software represents the amount of dose delivered by each beam for pre-specified time duration. Thus in the simulation framework, at each discrete time step, the collision between the voxels of the tumor and the dose matrix cube is computed. Once the colliding dose matrix cube is computed, the dose in the tumor voxel is added with the dose from that dose matrix cube divided by the total number of time steps. The collision of the dose matrix with the moving tumor is initially computed using a level-set based binary search algorithm. As the lung tumor moves as discussed in Section III-C, the collision of the dose matrix with the moving tumor is computed by searching for the closest neighbor to the initial collision result.

2) Dose Accumulation Representation: The dose accumulation is typically color coded either in grey-scale and color-scale. Using grey-scale the dose accumulated is normalized based on the film dosimetry calibration. In color-scale, the dose accumulated is normalized between blue, red and white: blue represents the less radiated area (0%–33% radiation), red represents the median of the radiated area (33%–66% radiation), and white represents the highly radiated region (66%–100% radiation).

G. Description of the ARC Display System

As discussed in Section II-B, while various 3D displays may be investigated for 3D lung tumor dosimetry, in this paper we investigate the feasibility of using the ARC display.

The ARC system consists of a head-worn projection display (HWPD) and a 3D tracker, A HWPD can be considered the smallest projector ever designed in the world. It has the unique property to be a see-through display with an optimized in weight 6 gram per eye custom projection optics that can achieve up to 90 degree field of view without an increase in weight for the optics. Furthermore in the HWPD, the location of the pupil is within the projection optics, which yields a distortion map that can be easily corrected or minimized. The display, which includes the projection optics, the micro displays, and the optomechanics, weighs less than 600 grams in the current prototype, which could be further optimized. The requirement for such HWPD is the use of retroreflective material placed in the environment that has the property to retro reflect the light to the user from which images are projected, It is the use of retroreflective material as opposed to conventional projection screen

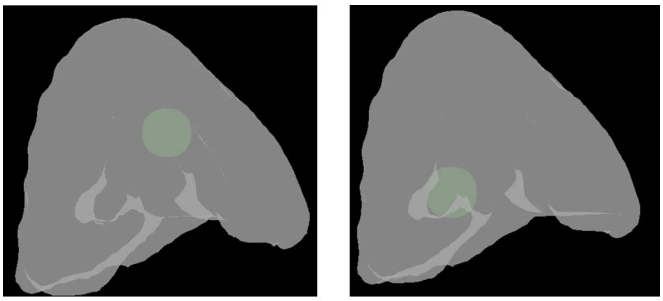

(a) (b)

Fig. 2. Spherical lung tumors at (a) upper and (b) lower lung.

that enables the HWPD to be the smallest ever designed projector, yet with sufficient illumination from each user point of view and no cross talk among users sharing a same visual space in a collaborative treatment planning exercise for example.

HWPDs take as input the simulation output from the computer and provide stereo visuals to the viewer [1]. The optical design of the visualization optics makes use of retroreflective material positioned in the environment to enable life-size rendition of the simulation output. The 3D tracker computes the 3D position of the viewer and enables the simulation program to account for the change in user's view position. When multiple users interact in the ARC, they naturally can see each other while also seeing the 3D dataset floating in space in front of them. Users can visualize different sides of the 3D dataset by either naturally walking around the data as if they would walk around a patient to see various sides of the anatomy, or being presented with a different view of the model as in many instances, physicians prefer to change the viewpoint. Also, multiple users may be given the same view of a dataset which is not achievable in volumetric 3D displays for example. Such capability can be desired in training or planning scenarios. The ARC display system enables users to navigate between various levels of immersion that occur on the basis of where users position themselves with respect to the retro-reflective material. The ARCs may take different shapes and sizes and are importantly deployable at different locations for different stages of the treatment planning and delivery. Variants of the HWPD optics targeted at specific applications such as 3D medical visualization and distributed AR medical training tools [23], embedded training display technology for military applications [24], and 3D manufacturing design collaboration [25] have been developed in our laboratory. The ARC system in summary provides unique capabilities such as: 1) spanning the virtuality continuum allowing both full immersion and mixed reality, which may open a set of new capabilities across various clinical applications (e.g. radiotherapy treatment planning and analysis); 2) enabling distributed interaction capability; and 3) creating small, low cost desktop technology or larger scale quickly deployable 3D visualization centers or displays.

IV. Results: Simulation of Lung Tumor Dosimetry

In this section, we present the results obtained from the simulation framework. We discuss two different simulation setups for visualizing the lung tumor motion in order to show the effect of the tumor's location and the breathing variations on the tumor dose accumulation. In the first setup, the 3D lung surface model was deformed with the ventilation signal given by a sinusoidal curve. In the second setup, the 3D lung surface model was deformed by providing the subject-specific ventilation signal from a strain gauge belt. The lung tumor was moved according to the motion of the lung surface model. Fig. 2 shows lung tumors at the upper [see Fig. 2(a)], and lower [see Fig. 2(b)] region of the lung. The tumor in the lower lung has a higher movement as compared to the tumor in the upper lung. Fig. 3 shows the upper lung tumor with the breathing cycle simulated using a sinusoidal curve [see Fig. 3(a)] and using the strain gauge signal collected from the patient [see Fig. 3(b)] taking into account the patient's ventilation and rib-cage movements. Fig. 3(c) shows the lower lung tumor with the breathing cycle simulated using a sinusoidal curve [see Fig. 3(c)] and using the strain gauge signal collected from the patient [see Fig. 3(d)]. It can be seen that the dose accumulation in lung tumor varies with the breathing pattern as well as the tumor location. Fig. 4(a) shows the ARC display system with the retro-reflective material placed on the wall. The user's view angle is tracked using an Intersense IS 1200 tracker with the miniature tracker camera mounted on the head-worn display and the marker fiducials placed in the ceiling. Fig. 4(a) also shows the lung tumor dose as displayed in the ARC display system. The promise is that clinicians can benefit from such simulation and display systems by better understanding the subject-specific dose accumulation in the moving lung tumor and its variations caused by location of the tumor and changes in the breathing pattern. What is unique about utilizing the ARC to visualize a patient's specific dosimetry estimation is the ability to display at life scale and to allow multiple users to naturally enter a 3D virtual world with 3D images of the patient anatomy and estimated datasets merged in one visualization dataset under discussion. Such visualization platform further facilitates team-work for treatment planning. The color capability and depth perception provided by the ARC system aims to facilitate a better understanding on the dose delivery levels to the lung as well as the dose-sensitive organs such as heart and esophagus. For instance, the inter-fractional changes in patient's breathing condition and the tumor shape leads to the exposure of cardiac region to the dose. The dose entering the cardiac region can be represented in a color coded manner and visualized effectively along with the 3D organ boundaries with the ARC system, and the treatment plan will be modified accordingly.

V. ARC System Evaluation for Lung Radiotherapy

We conducted a series of three experiments on the usage of the ARC system in visualizing the lung tumor radiotherapy simulation in real-time. In the first experiment, we evaluated the depth perception obtained using the ARC system in visualizing a given 3D data, and compared it to the depth perception obtained using a 2D monitor (MacBookPro laptop monitor @ resolution 1680×1050). In the second and third experiments, we focused on the visual perception of the spatial relations in the 3D volume rendered scene consisting of a deforming surface lung model and the tumor dose accumulation. In the second experiment, we aimed to find which of the two display hardware provides the fastest means to access the 3D dose accumulation in the moving tumor. Specifically, a question of interest is which display system (i.e., a 2D monitor versus the ARC display) can

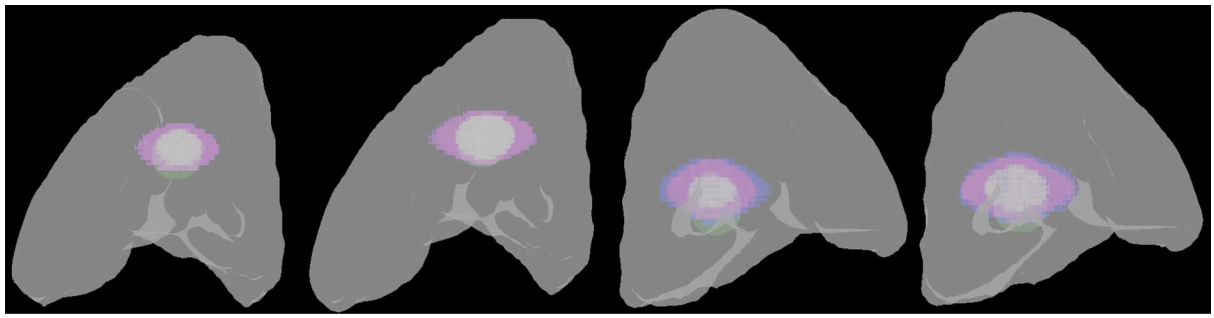

(a) (b) (c) (d)

Fig. 3. Radiation dose accumulation for the tumor at the upper lung with: (a) sinusoidal breathing and (b) subject-specific breathing signal. Radiation dose accumulation for the tumor at the lower lung with: (c) sinusoidal breathing and (d) subject-specific breathing signal.

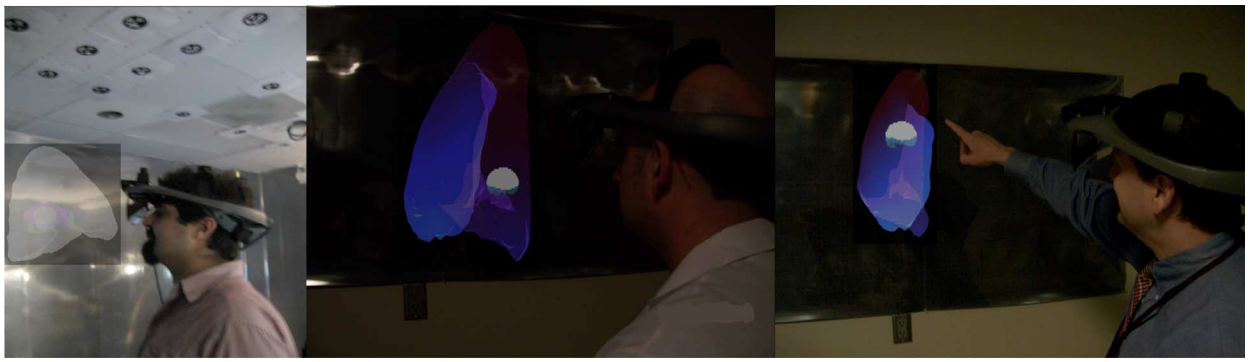

(a) (b) (c)

Fig. 4. ARC display system is shown (a) with the room covered with the retro-reflective material and the ceiling covered with the marker fiducials for tracking and the camera based tracker attached to the HMPD. Dose accumulation inside the lungs is visualized through the ARC system by radiation oncology experts in (b) and (c).

help experts most efficiently correlate the 3D dose delivered to a moving tumor, together with understanding the tumor movement path that is differentiated by the local elastic property. Experts can make sure that lung tumors located in regions of high elasticity, which reflects on healthy tissue around a tumor, are targeted with high dose accumulation on the tumor exclusively. In the clinical workflow, experts can use this visualization to re-plan the dose delivery in order to optimize the dose accumulation on the tumor. This visualization also allows the experts to decide whether a respiratory gating system is required for the dose delivery. In the third experiment, we extend the second experiment for fast detection of radiation hot spots inside and outside the lung. In the clinical workflow, experts can use this visualization as a patient treatment-delivery monitoring tool and abort the treatment when the hot spots are seen in the radiation sensitive areas such as the spinal cord or the cardiac region. A set of six radiation oncology experts was considered for this three-experiment evaluation. The experts were allowed to rotate the 3D scene to perceive the content in any of the experiments. It is to be understood that rotating the 3D model requires additional time for the experts to make their decision based on the perceived 3D content. For all the three experiments, the 3D scene was rotated at regular time intervals of one half second and in steps of 5 deg in the XZ plane along the anti-clockwise direction. The three experiments were carried as follows.

A. First Experiment

A 3D sphere and a 3D plane both rendered as a white wire mesh were used in the 3D scene without any overlap in their positions. The experts were asked to determine the 3D object that was closer to their viewpoint either using the HWD first and then the monitor or the reverse, which was selected randomly. When the viewpoint was rotated, the time spent rotating the 3D scene by each of the clinical experts in deciding as to which stimulus is closer to them was recorded. The experiment was repeated for 10 different combinations of the sphere and the plane positions. In each of the combinations, the dimensions of the sphere and the plane were varied. The results, tabulated in Table I, clearly indicate that the experts were able to perceive the 3D depth using the HWD directly without any significant rotation. The experts however took an average of 2.9 s to perceive the 3D depth of the content by 3D scene rotation when viewed through the monitor. While the experts can use the ARC system to perceive the 3D content of a simplistic scene slightly faster, of most importance was the fact that all experts had appropriate depth perception with either display.

B. Second Experiment

We first rendered the surface lung model as a translucent 3D model using alpha blending. The lung surface nodes were colored based on their local elasticity value represented by the normalized C_i value for each node i computed in Section III-B. The nodes were colored as red where the normalized C_i was zero and blue where the normalized C_i value was one. From a 3D rendering perspective, the red color value of each node was set to a minimum nonzero value. The green color value of each node was set to 0. The blue color value of each node i was set to be the normalized C_i value computed in Section III-B. The

TABLE I
COMPARISON OF THE ARC SYSTEM WITH THE 2D DISPLAY SYSTEM

Subject	Average time (sec) Experiment 1		Average time (sec) Experiment 2		Average time (sec) Experiment 3	
	ARC	2D monitor	ARC	2D monitor	ARC	2D monitor
Expert 1	0	2.55	0.75	11.05	1.05	13.05
Expert 2	0	0.95	1.05	8.95	0.95	11.0
Expert 3	0.45	4.05	0.95	12.05	1.55	15.05
Expert 4	0	3.95	0.55	14.95	1.05	14.05
Expert 5	0.55	2.55	1.45	8.0	0.9	16.0
Expert 6	0	3.45	1.40	9.0	1.55	13.0
Average	**0.2**	**2.9**	**1.0**	**10.7**	**1.2**	**13.7**

tumor volume was then rendered without the spherical mesh around its volume. For simplicity, the region inside the tumor, which received the 90%–100% of the prescribed dose was colored in white and the region inside the tumor, which received the 80%–90% of the prescribed dose was colored in green. The experts were asked to visualize the dose accumulation on the moving tumor and were asked to determine if the tumor was closer to the red surface region or the blue surface region of the lung surface model at the start of the inhalation. Fig. 4(b) and 4(c) shows experts visualizing the experiment using the ARC system. The experiment was repeated for 10 different combinations of the tumor position and tumor size inside the lung. In each of the cases, the lung tumor was displaced as previously discussed in Section III-C. The subjects reported 100% correct responses, however, they used different times to report as measured by the time spent in rotating the 3D scene. The results tabulated in Table I clearly indicate that the experts were able to tell where the tumor was located inside the lung with an average time of 1 second. The experts took an average time of 10.7 s to perceive the 3D depth of the content when viewed through the monitor. Because when applied to real time radiotherapy, the individual dose beams are delivered to the patient in 30–40 s, a 10-s delay in decision-making is a significant amount of time in the assessment of dose accumulation. This experiment shows that oncology experts can use the ARC system to make fast decisions during treatment re-planning.

C. Third Experiment

We evaluated the role played by the 3D display system in enabling the expert to detect radiation hot spots both inside and outside the lung. We extended the second experiment by exposing the radiation dose to a 3D location both inside and outside the lung. The same color-coding scheme used in the second experiment was also used in this experiment. The experiment was repeated for ten different combinations of the hot-spot position and size. The subject reported 100% correct responses, however they used different times to report as measured by the time spent in rotating the 3D scene. The results, tabulated in Table I, clearly indicate that the experts were able to tell where the hot spot was located inside the lung with an average time of 1.2 s. However, when the hot spot was near the spinal cord region, the experts viewing the 3D scene in the HWD rotated the model to better understand the position of the hot spot. The experts took an average time of 13.7 s to perceive the 3D depth of the content when viewed through the monitor. This experiment shows that oncology experts can effectively use the 3D ARC system to quickly detect hot spots inside or outside the lung. In the clinical workflow, the experts will be able to abort the dose delivery in order to reduce irradiating sensitive organs such as Spinal cord.

VI. DISCUSSION

The method for simulating lung tumor motion and its dosimetry and displaying the lung tumor dose accumulation in a 3D display system allows oncologists to have the ability to visualize 3D radiation doses depositing during the process of radiation therapy delivery. Such visualization allows appreciating discrepancies in actual delivery. The framework, for the first time enables visualizing the 3D dose accumulation on a moving tumor.

The display system used for visualizing this simulation framework is a stereoscopic HWPD system. While other 3D display systems can also be used with the simulation framework, the ARC based display system. Custom designed and built in our laboratory, ARC display system was chosen for its high resolution of 2.4 arcmin, color capability, scalability, mobility and multiuser collaboration capability, all essential for the proposed simulation framework. An evaluation of this framework using six clinical experts was discussed in Section V of this paper. Results show that the clinicians were able to use the display system to monitor the radiation dose delivery on the tumor and also the generation of hot spots outside the lung, efficiently. The color capability and the depth perception provided by the ARC system enabled them to perceive the 3D content without the need to rotate the viewpoint, thereby enabling faster decisions to be made during treatment monitoring. The experts with the local tissue properties also correlated a 3D simulated hot spot's location. In the clinical workflow, the experts will also able to decide whether to abort the delivery based on the 3D location of the hot spot formation.

In this paper, the simulation framework and dose model that have been described constitute a first-order estimation of the dose because the model assumes that the tissues within the simulation framework are of uniform density. Future work will include correlating clinical outcomes to dosimetric information. Also, future work will involve deformation of the dose grid extracted from the Brainlab to reflect the changes in the radiation dose caused by the dose scattering induced by the moving tissue. This work will involve even more accurate dose computation algorithms and a Monte Carlo algorithm to accurately account for the dose differences associated with the various density differences of normal lung and target tissue.

The usage of rendering techniques and optimizations that provide an improved 3D perception of the rendered anatomical model as well as the dose accumulation are under development and investigation. The proposed visualization and display system is aimed at real time therapeutic approaches that will include adjustments of treatment inaccuracies. Although the current paper describes a process that is specific to radiation therapy, the simulation and display technology could be applied to other noninvasive treatment techniques such as cryotherapy, radiofrequency ablation or high intensity ultrasound. Apart from lung cancers, the technique could clearly be applied to different anatomic sites, with the ability to tailor the output to idiosyncrasies of these different anatomic sites.

REFERENCES

[1] J. P. Rolland, F. Biocca, F. Hamza-lup, Y. Ha, and R. Martins, "Development of head-mounted projection displays for distributed collaborative augmented reality applications," *Presence: SI Immersive Projection Technol.*, vol. 14, no. 5, pp. 528–549, 2005.

[2] M. van Herk, "Errors and margins in radiotherapy," *Seminaire on Radiation Oncol.*, vol. 14, no. 1, pp. 52–64, 2004.

[3] D. A. Low, M. Nystrom, E. Kalinin, and P. Parikh, "A method for the re-construction of four dimensional synchronized CT scans acquired during free breathing," *Med. Phys.*, vol. 30, no. 6, pp. 1254–1263, 2003.

[4] D. A. Low, P. J. Parikh, W. Lu, J. F. Dempsey, S. H. Wahab, J. P. Hubenschmidt, M. M. Nystrom, M. Handoko, and J. D. Bradley, "Novel breathing motion model for radiotherapy," *Int. J. Rad. Oncol Biol. Phys.*, vol. 63, no. 3, pp. 921–929, 2005.

[5] W. Lu, K. J. Ruchala, M.-L. Chen, Q. Chen, and G. Olivera, "Real-time respiration monitoring using the radiotherapy treatment beam and four dimensional computed tomography (4DCT)—A conceptual study," *Phys. in Medicine and Biol.*, vol. 51, pp. 4469–4495, 2006.

[6] I. J. Chetty, M. Rosu, N. Tyagi, L. H. Marsh, D. L. McShan, J. M. Balter, B. A. Fraass, and R. K. Ten Haken, "A fluence convolution method to account for respiratory motion in three-dimensional dose calculations of the liver: A Monte Carlo study," *Med. Phys.*, vol. 30, no. 7, pp. 1776–1780, 2003.

[7] P. J. Keall, G. S. Mageras, J. M. Balter, R. S. Emery, K. M. Forster, S. B. Jiang, J. M. Kapatoes, D. A. Low, M. J. Murphy, B. R. Murray, C. R. Ramsey, M. B. Van Herk, S. S. Vedam, J. W. Wong, and E. Yorke, "The management of respiratory motion in radiation oncology report of AAPM Task Group 76," *Med. Phys.*, vol. 33, no. 10, pp. 3874–3900, 2006.

[8] T. Pan, T. Y. Lee, E. Rietzel, and G. T. Chen, "4D-CT imaging of a volume influenced by respiratory motion on multi-slice CT," *Med. Phys.*, vol. 31, no. 2, pp. 333–340, 2004.

[9] M. Schaefer, M. W. Munter, C. Thilmann, F. Sterzing, P. Haering, S. E. Combs, and J. Debus, "Influence of intra-fractional breathing movement in step-and-shoot IMRT," *Phys. in Medicine and Biol.*, vol. 49, no. 12, pp. N175–N179, 2004.

[10] S. A. Naqvi and W. D. D'Souza, "A stochastic convolution/superposition method with isocenter sampling to evaluate intrafraction motion effects in IMRT," *Med. Phys.*, vol. 32, no. 4, pp. 1156–1163, 2005.

[11] W. D. D'Souza, S. A. Naqvi, and C. X. Yu, "Real-time intra-fraction-motion tracking using the treatment couch: A feasibility study," *Phys. in Medicine and Biol.*, vol. 50, no. 17, pp. 4021–4033, 2005.

[12] B. Kanagaki, P. W. Read, J. A. Molloy, J. M. Larner, and K. Sheng, "A motion phantom study on helical tomotherapy: The dosimetric impacts of delivery technique and motion," *Phys. in Medicine and Biol.*, vol. 52, no. 1, pp. 243–255, 2007.

[13] R. Kashani, K. Lam, D. Litzenberg, and J. M. Balter, "Technical note: A deformable phantom for dynamic modeling in radiation therapy," *Med. Phys.*, vol. 34, no. 1, pp. 199–201, 2007.

[14] J. Geng, "Volumetric 3D display radiation therapy planning," *IEEE J. Display Technol.*, vol. 4, no. 4, Dec. 2008.

[15] O. Cakmakci and J. P. Rolland, "Head-worn display," *IEEE J. Display Technol.*, vol. 2, no. 3, pp. 199–216, Sep. 2006.

[16] J. P. Rolland, O. Cakmakci, J. Covelli, C. Fidopiastis, F. Fournier, R. Martins, F. Hamza-lup, and D. Nicholson, "Beyond the desktop: Emerging technologies for supporting 3D colloborative teams," *Int. J. Interact. Des. Manuf.*, vol. 4, no. 1, pp. 239–241, 2007.

[17] F. Hamza-lup, A. Santhanam, C. Imielinska, S. L. Meeks, and J. P. Rolland, "Distributed augmented reality with 3D lung models—A planning tool concept," *IEEE Trans. Inf. Technol. Biomed.*, vol. 11, no. 1, pp. 40–46, Mar. 2007.

[18] O. Cakmakci and J. P. Rolland, "Design and fabrication of a dual-element off-axis near-eye optical magnifier," *Opt. Lett.*, vol. 32, no. 11, pp. 1363–1365, 2007.

[19] A. Santhanam, S. P. Mudur, and J. P. Rolland, "An inverse 3D lung deformation analysis for medical visualization," in *IEEE Computer Graphics Soc. Computer Animation and Social Agents (CASA)* , Geneva, Switzerland, 2006, pp. 229–242.

[20] A. Santhanam, C. Imielinska, P. Davenport, P. Kupelian, and J. P. Rolland, "Modeling and simulation of real-time 3D lung dynamics," *IEEE Trans. Inf. Technol. Biomed.*, vol. 12, no. 2, pp. 257–270, 2008.

[21] A. Santhanam, "Modeling Simulation and Visualization of 3D Lung Dynamics," PhD Dissertation, College of engineering and computer science, Univ. Central Florida, Orlando, 2006.

[22] D. H. Griffel, *Applied Functional Analysis*. New York: Dover , 2002.

[23] J. P. Rolland, F. Hamza-lup, L. Davis, J. Daly, Y. Ha, G. Martin, J. Norfleet, R. Thumann, and C. Imielinska, "Development of a training tool for endotracheal intubation: Distributed augmented reality," in *Medicine Meets Virtual Reality*, Newport beach, CA, 2003, pp. 288–294.

[24] A. Rodriguez, M. Foglia, and J. P. Rolland, "Embedded training display technology for the army's future combat vehicles," in *Proc. 24th Army Sci. Conf.*, Orlando, FL, 2003, pp. 1–6.

[25] J. P. Rolland, F. Biocca, H. Hua, Y. Ha, C. Gao, and O. Harryson, "Teleportal augmented reality system: Integrating virtual objects, remote collaborators, and physical reality for distributed networked manufacturing," in *Virtual and Augmented Reality Applications in Manufacturing*, K. Ong and A. Y. C. Nee, Eds. London: Springer-Verlag, 2004, pp. 179–200.

Anand P. Santhanam (S'04–M'05) received the Masters degree from the University of Texas, Dallas, in 2001, and the Ph.D. degree from the University of Central Florida in 2006, both in computer science.

He was a software engineer for Nortel Networks from April 2000 to January 2001 and Metera Networks from February 2001 to January 2002. From 2006 to 2008, he was a Post-Doctoral associate in the M.D. Anderson Cancer Center Orlando and the College of Optics and Photonics at the University of Central Florida. He is currently a research scientist at the College of Optics and Photonics, University of Central Florida, Orlando.

Dr. Santhanam received a 2005 Link Foundation Fellowship award for his research.

Twyla R. Willoughby received the Masters degree in medical physics from the Graduation School of Biomedical Science, University of Texas, in 1995.

Since her graduation, she has worked as a clinical medical physicist. Her previous work includes commissioning radiosurgical systems for brain radiosurgery, commissioning and treatment planning of IMRT treatment, and startup of various image guidance treatment techniques including ultrasound, daily MV CT, and daily radiography. She is currently with MD Anderson Cancer Center Orlando, Orlando, FL.

Ilhan Kaya received the Masters degree in computer science from Bogazici University, Istanbul, Turkey, in 2004. He is currently working toward the Ph.D. degree from the School of Electrical Engineering and Computer Science, University of Central Florida, Orlando.

He was a software engineer in Finansbank, Istanbul, Turkey, from 2000 to 2003, and with Telenity, Istanbul, Turkey, from 2004 to 2005. He was a software intern for the AMD graphics, Orlando, FL, from 2008 May to 2008 August.

Amish P. Shah received the Ph.D. degree in biomedical engineering from the University of Florida, Orlando, in 2004.

His research was focused on the revision of radiation dose estimates to red bone marrow from radionuclide therapies for cancer. He then completed a residency in radiation therapy physics at MD Anderson Cancer Center Orlando, Orlando, FL, in 2007, where he is currently a clinical and research medical physicist.

Sanford L. Meeks received the B.S. degree in physics from Florida Southern College, the M..S. degree in physics from Florida State University, and the Ph.D. degree in medical physics from the University of Florida in 1994.

He currently serves as the Chief of Physics at MD Anderson Cancer Center Orlando, Orlando, FL. He joined the faculty at the University of Florida in 1995 and held appointments in the Departments of Neurological Surgery, Radiation Oncology, and Nuclear and Radiological Engineering. In 1999, he joined the Department of Radiation Oncology at the University of Iowa as Associate Professor and Director of Medical Physics, and he held a secondary appointment in the Department of Biomedical Engineering.

Jannick P. Rolland (SM'08) received the Masters degree from the Institut D'Optique, Graduate School, France, in 1984, and the Ph.D. degree in optical science from the University of Arizona in 1990.

She joined the Research Faculty at the University of Noreth Carolina at Chapel Hill in 1992, and headed the Vision Research Group (1992–1996). She is currently a Professor of Optics at the University of Central Florida, Orlando, with joint appointments in the College of Medicine and the College of Engineering.

Prof. Rolland received a UCF 2001 Distinguished Researcher Award, a 2006 Award for Excellence in Teaching, and a 2007–2012 Florida Photonics Center for Excellence Professorship. She is a Fellow of the Optical Society of America (OSA) and the SPIE, and a member of the Society for Information Display (SID).

Patrick A. Kupelian received the M.D. degree from The American University of Beirut Medical Center, Beirut, Lebanon. He completed his residency in radiation oncology at the University of Texas M.D. Anderson Cancer Center, Houston, TX, and a fellowship in radiation oncology of genitourinary malignancies at the Cleveland Clinic Foundation, Cleveland, OH.

After serving as Clinical Research Director, Department of Radiation Oncology at the Cleveland Clinic Foundation from 1999 to 2002, he joined the MD Anderson Cancer Center Orlando, Orlando, FL, where he is Director of Research for Radiation Oncology.

Dr. Kupelian is a member of the American Society for Therapeutic Radiology and Oncology, the European Society for Therapeutic Radiology and Oncology, the American Society of Clinical Oncology, the American Urological Association, and the American Brachytherapy Society.